Type-I superconductivity in single-crystal Pb_2Pd

Arushi,[1] K. Motla,[1] A. Kataria,[1] S. Sharma,[2] J. Beare,[2] M. Pula,[2] M. Nugent,[2] G. M. Luke,[2,3] and R. P. Singh[1,*]

[1]*Department of Physics, Indian Institute of Science Education and Research Bhopal, Bhopal 462066, India*

[2]*Department of Physics and Astronomy, McMaster University, Hamilton, Ontario L8S 4M1, Canada*

[3]*TRIUMF, Vancouver, British Columbia V6T 2A3, Canada*

(Received 19 January 2020; revised 29 April 2021; accepted 3 May 2021; published 13 May 2021)

We have investigated the superconducting properties in a single crystal of the superconductor Pb_2Pd via various techniques including, magnetization, AC transport, transverse field muon spin rotation and relaxation, and heat capacity. All measurements confirm the superconducting transition temperature $T_C = 3.0 \pm 0.1$ K. Electronic specific-heat data are well described by the BCS expression, suggesting that Pb_2Pd opens an isotropic gap on entering the superconducting state. Specific-heat jump and the $\lambda_{e\text{-}ph}$ value categorize Pb_2Pd as a moderately coupled superconductor. Magnetization and transverse field muon spin rotation measurements along with the Ginzburg-Landau parameter, $\kappa < 1/\sqrt{2}$ demonstrates that Pb_2Pd is a type-I superconductor.

DOI: 10.1103/PhysRevB.103.184506

I. INTRODUCTION

In recent years, the discovery and study of exotic phases of matter, such as Weyl and Dirac semimetals [1], topological insulators [2], and topological superconductors [3] continues to interest both theorists and experimentalists. Among these phases, topological superconductivity (TSC) is one of the most studied phenomena and has become a rapidly developing field in which significant advances have been recently made [3]. It not only enriches the existing theoretical framework of physics, but also provides a background for investigations on low-energy excitations, Majorana fermions which have potential applications in fault-tolerant quantum computation [4,5]. Apart from computation applications, TSC itself is an intriguing topological phase of matter, namely, a new type of unconventional superconductivity. In order to realize a topological superconducting state, strong spin-orbital coupling (SOC) is considered one of the necessary ingredients [6]. Superconducting compounds containing heavy atomic number (Z) elements are known to have strong SOC since the strength of SOC is proportional to Z^4. These superconducting systems with strong SOC often show various exotic properties, such as robustness of superconductivity beyond the Pauli limit [7–9], nodes and multiple gaps in the superconducting state [10–12], time-reversal symmetry breaking [13–15], as well as being a platform to realize topological superconductivity. Intrinsic topological superconductivity is still a rare phenomenon, although various methods have been employed in its study.

To date, Pb-rich compounds have not been investigated as potential candidates to exhibit exotic superconducting features, although they display a range of other interesting electronic properties. Recent work on some of the Pb-rich compounds (MPb_2 where M = Au, Rh, and Er) predicted them to be Dirac semimetals, topological superconductors, and display a coexistence of superconductivity with antiferromagnetic order, respectively [16–19]. The existence of topological phases of matter in Pb-rich compounds motivates us to study the superconducting and normal-state properties of a theoretically proposed topological material Pb_2Pd [20].

In this paper, we report the superconducting properties in a single crystal of Pb_2Pd which demonstrate type-I superconductivity. Until now, this feature remained unexplored, although superconductivity has been known in this compound since 1962 [21]. This behavior is surprising because only a few binary [22–29] and ternary compounds [30–32] are known to exhibit type-I superconductivity. Electrical transport, magnetization, and specific-heat measurements confirm bulk superconductivity below the transition temperature $T_C = 3.0 \pm 0.1$ K. To confirm the type-I nature of superconductors, a microscopic technique known as muon spin rotation and relaxation (μSR) was considered as a powerful tool in recent years and has been employed for various superconductors [27–29,31–33]. For Pb_2Pd as well, μSR and magnetization measurements were used to find the nature of superconductivity, and both measurements confirmed the type-I behavior. Specific-heat measurement indicates a moderate electron-phonon coupling.

II. EXPERIMENTAL DETAILS

A polycrystalline sample of Pb_2Pd was synthesized by adding starting materials Pb and Pd in a ratio of 2:1 in an evacuated sealed quartz tube. It was then heated beyond the melting point (°C). A single crystal was prepared by the Bridgman technique in which the polycrystalline sample was placed in a conical quartz ampoule, heated to 570 °C, dwelled for 30 h and then slowly cooled to 456 °C, followed by water quenching. Phase purity and crystal structure characterization were performed using a Cu $K\alpha$ (1.5406 Å)-equipped PAN analytical powder x-ray diffractometer. The orientation and single-crystal nature of our crystals were determined using a white beam x-ray-diffraction (XRD) Laue instrument. The data was collected using NORTH STAR software. Magnetization and AC susceptibility measurements were carried out in a range of 1.8–10 K and 0–30 mT using a Quantum Design

*rpsingh@iiserb.ac.in

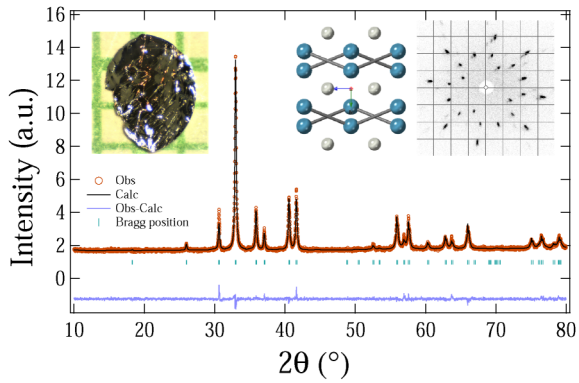

FIG. 1. The powder XRD pattern of Pb_2Pd obtained at room temperature is shown by red circles whereas the black line represents the Rietveld refinement. The crystal image (left-up) and crystal structure of Pb_2Pd where blue circles represent Pb atoms, whereas gray circles represent a Pd atom (right-up). The back Laue x-ray diffraction pattern of a Pb_2Pd single crystal (rightmost).

magnetic property measurement system. Electrical resistivity using a four-probe AC technique in the range of 1.9–300 K and specific-heat (two-τ relaxation method) measurements were performed on a Quantum Design physical property measurement system.

Transverse field muon spin rotation (TF-μSR) measurements were carried out to investigate the magnetic-field distribution inside the sample. The data were collected using the M15 beamline at TRIUMF, Centre for Molecular and Material Science, Vancouver, Canada. The spectrometer incorporates a dilution refrigerator which allows for measurements from 0.02 to 2.8 K (for our case) and has a time resolution of 0.4 ns. The single-crystal sample used for our measurement was cut into plates before mounting on the cold finger so that a large fraction of the muon beam is covered. In TF geometry, the magnetic field was applied parallel to the direction of the muon beam with the initial muon spin arranged perpendicular to the field. The direction of the applied magnetic field was perpendicular to the c axis of the crystal. The μSRFIT software package was used to analyze the μSR data [34].

III. RESULTS AND DISCUSSION

A. Crystal structure characterization

Room-temperature XRD pattern on powdered crystals is shown in Fig. 1. Rietveld refinement confirms the phase purity and crystal structure as a body-centred tetragonal with space-group $I4/mcm$. The obtained lattice parameters are as follows: $a = b = 6.859$ and $c = 5.838$ Å [35]. All parameters including atomic and Wyckoff positions, cell volume, etc., obtained from refinement, are summarized in Table I. Figure 1 (right) also shows the Laue pattern where the symmetric and bright spots indicate the single-crystalline nature of Pb_2Pd and correspond to the (001) growth direction.

B. Normal- and superconducting state properties

Figure 2 shows the electrical resistivity of Pb_2Pd as a function of temperature obtained at the zero field in the range

TABLE I. Parameters obtained from Rietveld refinement.

Structure space-group lattice parameters	Tetragonal $I4/mcm$			
$a = b$ (Å)	6.859(3)			
c (Å)	5.838(3)			
Atom	Wyckoff position	x	y	z
Pd1	4a	0	0	0.250
Pb1	8h	0.165	0.665	0

of 1.9–300 K. The inset shows a drop in resistivity at a temperature $T_{c,\text{onset}} = 3.0 \pm 0.1$ K with a transition width $\Delta T = 0.1$ K which confirms superconductivity in this compound. The residual resistivity ratio $= \rho$ (300 K)$/\rho$ (6 K) $= 19$ and the low value of ρ_0 imply a low amount of disorder in the present sample. The saturating-type behavior of $\rho(T)$ instead of linear T dependence at high temperatures, allows these data to be fit by the parallel resistor model. This possibility arises when the order of mean free path becomes short, equal to a few interatomic spacing [36]. In such a case, the scattering cross section will no longer be linear in the scattering perturbation. This leads to electron-phonon-type interactions being the dominant scattering mechanism at higher temperatures. Hence, the resistivity will rise less rapidly with temperature showing a saturating behavior. This type of behavior in $\rho(T)$ was described by Wiesmann *et al.* [37] by the following expression:

$$\rho(T) = \left[\frac{1}{\rho_s} + \frac{1}{\rho_i(T)}\right]^{-1}, \quad (1)$$

where ρ_s is the temperature-independent saturation resistivity attained at higher temperatures and $\rho_i(T)$ is given by

$$\rho_i(T) = \rho_{i,0} + C\left(\frac{T}{\Theta_D}\right)^5 \int_0^{\Theta_D/T} \frac{x^5}{(e^x - 1)(1 - e^{-x})} dx, \quad (2)$$

where $\rho_{i,0}$ represent temperature-independent residual resistivity due to scattering from defects in the crystal

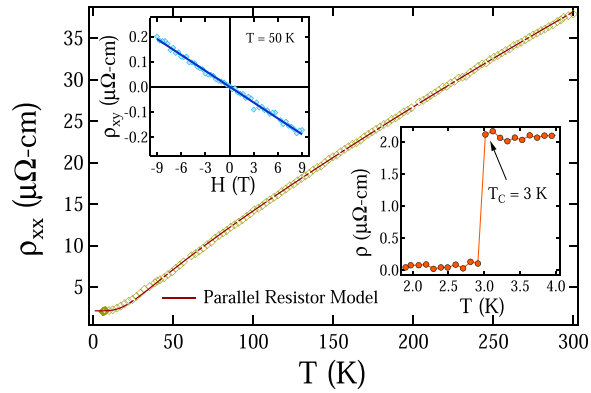

FIG. 2. Zero-field temperature variation of electrical resistivity in the range of 1.9 K $\leqslant T \leqslant$ 300 K where the solid red line is a fit to the parallel resistor model. The inset (bottom right): A sharp superconducting transition at $T_C = 3.0$ K whereas the top left inset shows the Hall resistivity with respect to field (±9 T) at $T = 50$ K.

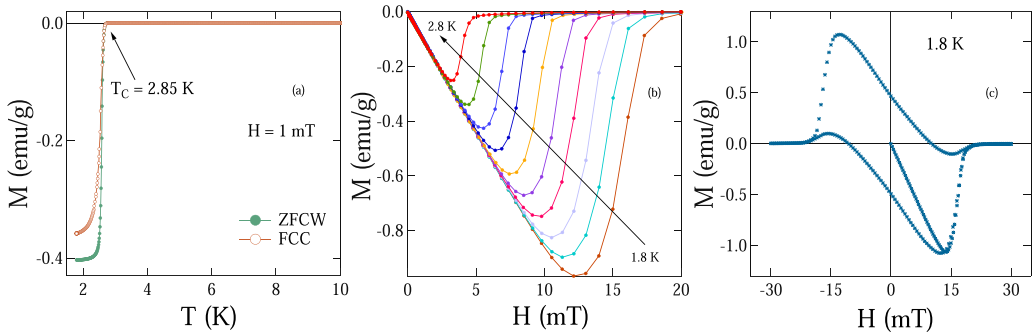

FIG. 3. (a) Temperature dependence of the moment collected via ZFCW and FCC under an applied magnetic field of 1 mT. (b) Magnetization as a function of applied field for 1.8 K $\leqslant T \leqslant$ 2.8 K. (c) Magnetization vs magnetic field at 1.8 K of Pb_2Pd.

structure whereas the second term is temperature-dependent generalized Bloch–Grüneisen (BG) resistivity in which C is a material-dependent quantity and Θ_D is the Debye temperature obtained from resistivity measurements. The red dashed line in Fig. 2 shows the best fit to the data and yields $\rho_0 = 2.14 \pm 0.03$, $C = 63 \pm 1$, $\rho_{0,s} = 378 \pm 12\ \mu\Omega\,\text{cm}$, and $\Theta_D = 116 \pm 2$ K which is close to Θ_D obtained from specific-heat measurement (discussed later).

In order to extract the information regarding the carrier density of Pb_2Pd, Hall resistivity, ρ_{xy} as a function of a magnetic field in the range of ± 9 T and at $T = 50$ K was measured as shown in the top left panel of Fig. 2. We have determined the normal-state Hall coefficient, and the R_H form the slope of a linear fit to the $\rho_{xy}(H)$ data in both field directions. The value obtained for $R_H = -(2.11 \pm 0.02) \times 10^{-10}\ \Omega\,\text{mT}^{-1}$ and the negative sign indicate towards the electron as the charge carriers. By using $R_H = -1/ne$, where n is the carrier density and e is the electronic charge, we obtained $n = (2.96 \pm 0.02) \times 10^{28}\ \text{m}^{-3}$. Theoretically, the carrier density is defined as $n = Z/V_{\text{cell}}$, where $Z = 8$ is the number of conduction electrons per unit cell and $V_{\text{cell}} = 0.275 \times 10^{-27}\ \text{m}^3$ for Pb_2Pd, yielding a value of $n = 2.90 \times 10^{28}\ \text{m}^{-3}$ and is close to the experimentally obtained value.

Magnetization measurements have been performed on the single crystal oriented along the (001) direction in both the parallel and the perpendicular magnetic-field configuration. It was obtained via two modes: zero-field-cooled cooling (ZFCW) and field-cooled cooling (FCC) under an applied magnetic field of 1.0 mT which confirms the superconducting nature of Pb_2Pd displayed in Fig. 3(a). A strong diamagnetic signal on entering the superconducting state at a transition temperature of $T_{c,\text{onset}} = 2.85 \pm 0.10$ K is observed, in agreement with the previous report [21,38]. There was no anisotropy in the observed T_C in both configurations, so the rest of the measurements were performed with the mag-

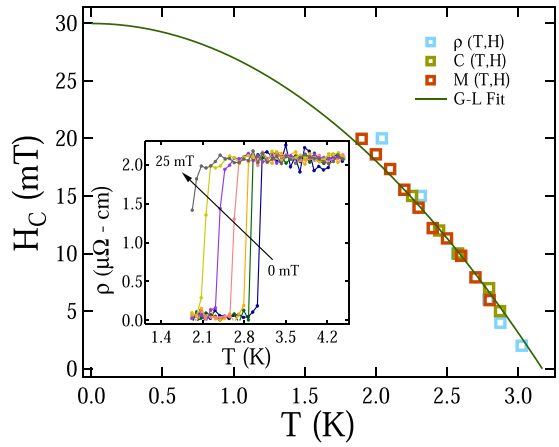

FIG. 4. Temperature dependence of the critical field from various measurements. The inset: $\rho(T)$ at different fields starting from 0 to 25 mT.

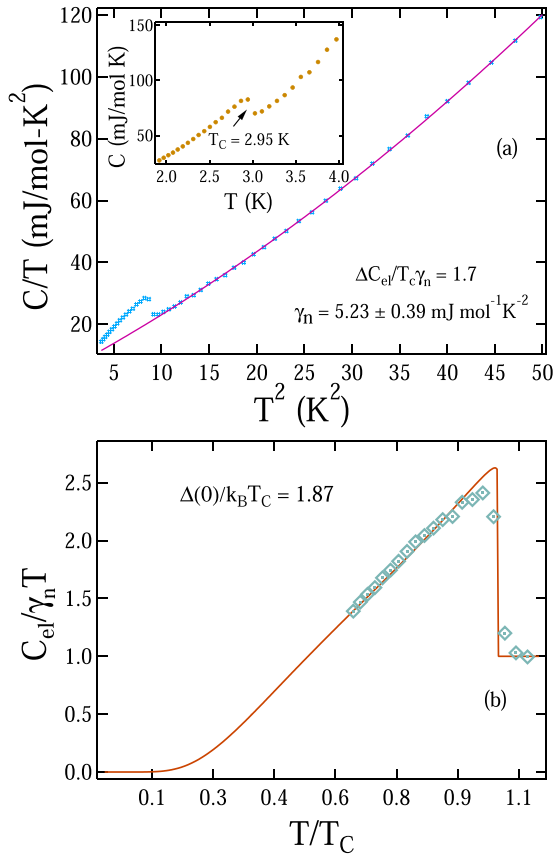

FIG. 5. (a) Zero-field C/T variation with respect to T^2 where the solid line represents a fit to $\frac{C}{T} = \gamma_n + \beta_3 T^2 + \beta_5 T^4$. Inset: Specific-heat data exhibiting a superconducting transition at $T_C = 2.95$ K. (b) s-wave fitting to the normalized electronic specific-heat data shown by the solid line.

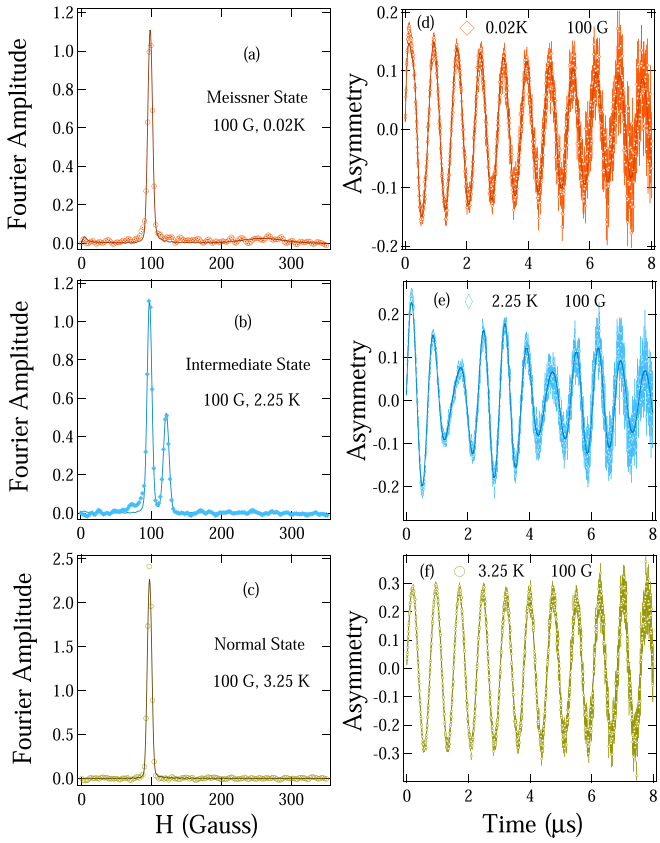

FIG. 6. The Fourier transform of μSR asymmetry representing the local field distribution and asymmetry spectra at different fields and temperatures. (a)–(c) show field distribution in the Meissner, intermediate, and normal state whereas (d)–(f) consists of corresponding asymmetry spectra. The solid lines are fit to the data using Eq. (5).

netic field perpendicular to the (001) direction. The Meissner volume fraction indicates the complete expulsion of flux in the superconducting state of this compound. Figure 3(c) represents the *M-H* curve obtained at 1.8 K where it exhibits a diamagnetic signal on reentering the superconducting state. This type of magnetic behavior is expected for type-I superconductors and has been observed in other type-I superconductors, including AuBe [28], Ir_2Ga_9 [39], and $LaRhSi_3$ [32]. The absence of a sharp transition to the normal state is accounted for the demagnetization factor. Low-field magnetization curves obtained for different temperatures [as shown in Fig. 3(b)] together with specific-heat and resistivity data at various fields are used to depict the critical field value at 0 K and fit according to

$$H_C(T) = H_C(0)\left[1 - \left(\frac{T}{T_C}\right)^2\right]. \tag{3}$$

The green solid curve shown in Fig. 4 represents the Ginzburg-Landau fit and the obtained value for $H_C(0) = 29.9 \pm 0.3$ mT.

Specific-heat measurements on the single crystal of Pb_2Pd were performed in the zero field from 1.9 to 10 K and are displayed in the inset of Fig. 5(a). The jump in the specific heat at $T_{c,\text{midpoint}} = 2.95 \pm 0.10$ K which is in agreement with the other measurements confirms the bulk nature of the superconductivity. Above the transition temperature, data are well described by $\frac{C}{T} = \gamma_n + \beta_3 T^2 + \beta_5 T^4$, shown by the solid pink line in Fig. 5(a) and yield a value of Sommerfeld coefficient $\gamma_n = 5.23 \pm 0.39$ mJ mol^{-1} K^{-2}, $\beta_3 = 1.65 \pm 0.03$ mJ mol^{-1} K^{-4}, and $\beta_5 = 0.0129 \pm 0.0005$ mJ mol^{-1} K^{-6}. The Debye temperature θ_D [40] is given by $(12\pi^4 RN/5\beta_3)^{1/3}$ where using $R = 8.314$ J mol^{-1} K^{-2}, $N = 3$, and $\beta_3 = 1.65 \pm 0.03$ mJ mol^{-1} K^{-4}, we have determined $\theta_D = 152 \pm 1$ K. Furthermore, the Sommerfeld coefficient is related to the density of states at the Fermi energy by $[\pi^2 k_B^2 D_C(E_F)/3]$ which yields $D_C(E_F) = 2.2 \pm 0.1$ states eV^{-1} f.u.$^{-1}$. The value of $\theta_D = 152 \pm 1$ and $T_{c,\text{midpoint}} = 2.95 \pm 0.10$ K are used to estimate $\lambda_{e\text{-}ph}$ using McMillan's relation given below [41],

$$\lambda_{e\text{-}ph} = \frac{1.04 + \mu^* \ln(\theta_D/1.45T_C)}{(1 - 0.62\mu^*)\ln(\theta_D/1.45T_C) - 1.04}, \tag{4}$$

where μ^* represents the screened repulsive Coulomb potential and usually taken to be 0.13, yielding $\lambda_{e\text{-}ph} = 0.67 \pm 0.08$ which is slightly higher than the other weakly coupled superconductors.

The electronic specific-heat (C_{el}) contribution has been calculated by subtracting the lattice and phononic contribution from the total specific-heat (C). The magnitude of specific-heat jump $\Delta C_{el}/\gamma_n T_C = 1.7$, which is higher than the BCS weak-coupling limit 1.43. The value of the same together with $\lambda_{e\text{-}ph}$ suggests a moderately coupled superconductivity in Pb_2Pd. The BCS expression [42] for the specific heat below and above T_C is described well with the normalized electronic specific-heat data as shown in Fig. 5(b) and gives a value of $\alpha = \Delta(0)/k_B T_C = 1.87$ which is also a bit higher than the BCS value of $\alpha = 1.76$. Thus, the electronic specific-heat data provide compelling evidence of a moderately coupled isotropic *s*-wave BCS superconductivity in Pb_2Pd.

We now evaluate various superconducting parameters: l (mean free path), λ_L, ξ_0, and κ. The residual resistivity value along with electron carrier density is used to estimate the electronic mean free path $l = v_F \tau$ [43] where v_F and τ are the Fermi velocity and the scattering time. Based on the Drude model, the Fermi velocity is given by $\hbar k_F/m^*$ and scattering time $\tau^{-1} = ne^2\rho_0/m^*$ where m^* is the effective mass and n is the carrier density. The Fermi wave vector is calculated by assuming a spherical Fermi surface, using the following relation $k_F = (3\pi^2 n)^{1/3}$, where $n = (2.96 \pm 0.02) \times 10^{28}$ m^{-3} was used and k_F is estimated to be 0.957 Å^{-1}. The Sommerfeld coefficient from the specific-heat ($\gamma_n = 5.23$ mJ mol^{-1} K^{-2}) and the carrier density are used to estimate the effective mass $m^* = (\hbar k_F)^2 \gamma_n/\pi^2 n k_B^2$ [43], and it provides a value of $2.59 m_e$. By using all the calculated values of n, m^*, ρ_0, and k_F, we determined $v_F = 4.29 \times 10^5$ ms^{-1} and $l = 638$ Å.

In order to distinguish between type-I or type-II superconductivity, we further investigate London's penetration depth (λ_L), BCS coherence length (ξ_0), and the Ginzburg-Landau parameter (κ_{GL}). The penetration depth $\lambda_L = (m^*/\mu_0 ne^2)^{1/2}$ is estimated to be 497 Å by using the value of $m^* = 2.59 m_e$ and $n = 2.96 \times 10^{28}$ m^{-3}. Within BCS theory, the coherence length (ξ_0) is given by $0.18\hbar v_F/k_B T_C$, yielding a value of

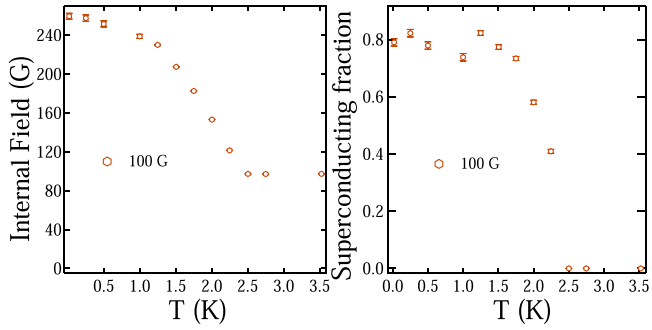

FIG. 7. (a) Internal field as a function of temperature in the normal region of Pb_2Pd. (b) Superconducting volume fraction with respect to temperature at a 100-G applied field.

2008 Å. The ratio $l/\xi_0 = 0.32$ concludes moderately dirty limit superconductivity in Pb_2Pd. The value of κ_{GL} distinguishes between a type-I and a type-II superconductor. In the dirty limit, κ_{GL} is given by $0.715\lambda_L(0)/l$ [43] which is found out to be 0.55, less than $1/\sqrt{2}$, classifies Pb_2Pd as a type-I superconductor. κ_{GL} is further determined using the relation $7.49 \times 10^3 \rho_0 \sqrt{\gamma}_{nV}$ and found out to be 0.56 by considering γ_{nV}, ρ_0 in cgs units, consistent with the value obtained before. To determine the Ginzburg-Landau coherence length $\xi(0)$ which is defined as $\lambda_{\text{eff}}/\kappa_{GL}$ where $\lambda_{\text{eff}} = \lambda_L(1 + \xi_0/l)^{1/2} = 1011.2$ Å. Considering γ_{nV}, ρ_0, and $\kappa_{GL} = 0.55$, $\xi(0)$ is evaluated to be 1817 Å.

A type-I superconductor generally exhibits three states: the Meissner, intermediate, and normal states, which can be distinguished according to the internal field distribution. The Meissner state corresponds to the complete superconducting region where all the applied magnetic field gets expelled from the inside of a superconductor. The intermediate state of a superconductor is characterized by the splitting of superconducting and normal regions when the applied magnetic field is less than the critical field. The intermediate state induced by the nonzero demagnetization effects causes some part of the superconductor (normal region) to experience a field greater than the applied field and equal to the critical field. Figure 6 shows the TF-μSR spectra and the corresponding internal field distribution in Pd_2Pd for all three states. The data was collected after field cooling the sample from the normal to the superconducting state in 100 G applied fields. The Fourier transform extracted from TF-μSR spectra provides information regarding the probability distribution of an internal field in the intermediate state of a type-I or a vortex state of a type-II superconductor. The presence of only a single peak at $H = H_{\text{app}} = 100$ G and $T = 0.02$ K corresponds to the Meissner state with the 100-G peak coming from the silver sample holder. Data taken at $T = 2.25$ K and $H_{\text{app}} = 100$ G corresponds to the intermediate state of Pb_2Pd with a peak at the applied field frequency from the sample holder, and a peak at a higher frequency corresponding to normal regions in the intermediate state. The asymmetry spectra were analyzed using the following equation:

$$A(t) = A_0[F(1 - F_S)\cos(\gamma_\mu H_N + \phi)\exp\left(-\frac{1}{2}\sigma_N^2 t^2\right) + (1 - F)\cos(\gamma_\mu H_{bg} + \phi)\exp(-\lambda_{bg} t)], \quad (5)$$

where A_0 is the initial asymmetry, F_S and F are the superconducting and total fraction coming from the sample, H_N is the internal field in the normal regions of the sample, H_{bg} is the contribution from the background field which originates due to muon stopping in the sample holder, ϕ is the phase shift, σ_N is the normal region relaxation rate, and λ_{bg} is the background relaxation rate. The fit using Eq. (5) at $T = 2.25$ K and $H = 100$ G provide two values of field: 100 and 123 G. The first value corresponds to the applied field whereas the second one is taken as an estimate of the critical field in the intermediate state of a type-I superconductor. Muons landing in the Meissner regions will not precess, whereas muons implanted in the normal region will precess with a magnetic-field $\sim H_C$. The Fourier transform shown in Fig. 6(b) consists of two peaks in which one peak at $H = 100$ G corresponds to the muon stopping in the silver cold finger as well as the normal-state regions of the superconductor whereas, the short peak centered at $H_{\text{int}} = 123$ G corresponds to the intermediate state in Pb_2Pd. This unambiguously demonstrates that Pb_2Pd is a type-I superconductor as the mixed state in a type-II superconductor will have a lower-field value than the applied field due to the establishment of flux line lattice.

The TF-μSR asymmetry spectra were also analyzed as a function of temperature for the applied 100-G field. Figure 7(a) shows the temperature dependence of the internal field in the normal region of Pb_2Pd. At $T \ll T_C$ and $H_{\text{app}} < H_C$, the internal field is equal to the critical field and as the temperature increases, it approaches the H_{app} value. The superconducting volume fraction with respect to temperature is shown in Fig. 7(b), and it shows an increasing behavior as the temperature decreases as it is expected for a type-I superconductor. The discrepancy observed between the $H_C(0)$ obtained from the muon and other measurements can be accounted due to the nonavailability of magnetization data below $T = 1.8$ K, which could have lead to the overestimation of the critical field using the Ginzburg-Landau fit.

To classify a superconductor as a conventional or unconventional, Uemura and co-workers [44–46] provide a classification based on their $\frac{T_C}{T_F}$ ratio. This ratio falls in the range of $0.01 \leqslant \frac{T_C}{T_F} \leqslant 0.1$ for many unconventional, such as heavy-fermion, iron-based superconductors, and high-T_C cuprates shown between the two blue solid lines. To calculate T_F for a 3D system, the following relation is used: $k_B T_F = (\hbar k_F)^2/2m^*$ where k_F is the Fermi wave vector. This gives $T_F = 13\,629$ K and the ratio $\frac{T_C}{T_F} = 0.000\,19$. It places Pb_2Pd away from the band of unconventional superconductors (as shown by a green symbol in Fig. 8). But at the same time, Pb_2Pd is also away from the type-I conventional superconductors, which are mostly pure elemental superconductors.

IV. CONCLUSION

In this paper, we have examined the superconducting properties of Pb_2Pd using specific heat, electric transport, magnetization, and TF-μSR measurements and found that it undergoes a sharp superconducting transition at $T_C = 3.0$ K. The value of residual resistivity, full Meissner fraction, and small width of superconducting transition in all measurements indicate towards the high sample purity and

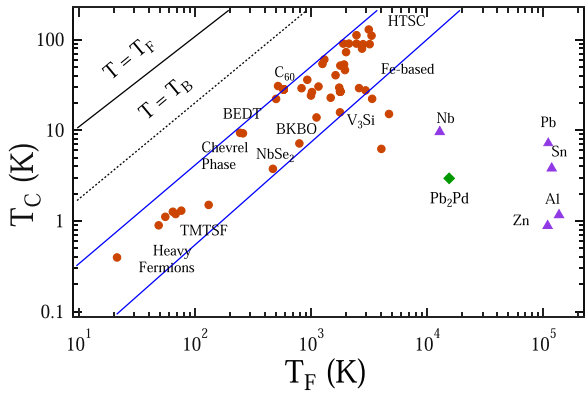

FIG. 8. The plot of Uemura and co-workers showing the superconducting transition temperature T_c vs the effective Fermi temperature T_F, where Pb_2Pd is shown as a solid red marker. Other data points plotted between the blue solid lines are the different families of unconventional superconductors [44–46].

crystallographic order. The field dependence of magnetization together with other superconducting parameters listed in Table II obtained from Sommerfeld coefficient and the residual resistivity value within the framework of BCS theory strongly revealed a type I and moderately dirty limit superconductivity in Pb_2Pd. Low-temperature specific-heat measurements suggest isotropic *s*-wave superconductivity with a moderate electron-phonon coupling. Our microscopic study of Pb_2Pd using TF-μSR measurement confirms type-I superconductivity. To establish a relation between the topological nature of the material and superconducting ground-state properties, further microscopic measurements need to be performed.

TABLE II. Superconducting and normal-state parameters of Pb_2Pd.

Parameters	Unit	Pb_2Pd
T_C	K	3.0 (1)
$H_C(0)$	mT	34 (1)
$\Delta C_{el}/\gamma_n T_C$		1.7 (1)
θ_D	K	152 (1)
$\lambda_{e\text{-}ph}$		0.7 (1)
$\Delta(0)/k_B T_C$		1.9 (2)
$\xi(0)$	Å	1817 (280)
m^*/m_e		2.6 (1)
n	10^{28} m^{-3}	2.96 (2)
l	Å	638 (60)
ξ_0	Å	2008 (220)
λ_L	Å	497 (20)
l/ξ_0		0.32
k_{GL}		0.55 (2)
v_f	10^5 ms^{-1}	4.3 (1)
T_F	K	13629
T_C/T_F		0.00019

ACKNOWLEDGMENTS

Arushi acknowledges the funding agency, University Grant Commission (UGC), Government of India for providing a SRF fellowship. R.P.S. acknowledges Science and Engineering Research Board, Government of India for the Core Research Grant No. CRG/2019/001028.

[1] N. P. Armitage, E. J. Mele, and A. Vishwanath, Rev. Mod. Phys. **90**, 015001 (2018).
[2] M. Z. Hasan and C. L. Kane, Rev. Mod. Phys. **82**, 3045 (2010).
[3] Y. Li and Z.-A. Xu, Adv. Quantum Technol. **2**, 1800112 (2019).
[4] J. Alicea, Y. Oreg, G. Refael, F. von Oppen, and M. P. A. Fisher, Nat. Phys. **7**, 412 (2011).
[5] X.-J. Liu, C. L. M. Wong, and K. T. Law, Phys. Rev. X **4**, 021018 (2014).
[6] M. Sato and Y. Ando, Rep. Prog. Phys. **80**, 076501 (2017).
[7] M. Uchida, M. Ide, M. Kawamura, K. S. Takahashi, Y. Kozuka, Y. Tokura, and M. Kawasaki, Phys. Rev. B **99**, 161111(R) (2019).
[8] N. Kimura, K. Ito, H. Aoki, S. Uji, and T. Terashima, Phys. Rev. Lett. **98**, 197001 (2007).
[9] E. M. Carnicom, W. W. Xie, T. Klimczuk, J. J. Lin, K. Górnicka, Z. Sobczak, N. P. Ong, and R. J. Cava, Sci. Adv. **4**, eaar7969 (2018).
[10] K. Maki, S. Haas, D. Parker, H. Won, K. Izawa, and Y. Matsuda, Europhys. Lett. **68**, 720 (2004).
[11] K. Izawa, Y. Nakajima, J. Goryo, Y. Matsuda, S. Osaki, H. Sugawara, H. Sato, P. Thalmeier, and K. Maki, Phys. Rev. Lett. **90**, 117001 (2003).
[12] Z. F. Weng, J. L. Zhang, M. Smidman, T. Shang, J. Quintanilla, J. F. Annett, M. Nicklas, G. M. Pang, L. Jiao, W. B. Jiang, Y. Chen, F. Steglich, and H. Q. Yuan, Phys. Rev. Lett. **117**, 027001 (2016).
[13] Y. Aoki, A. Tsuchiya, T. Kanayama, S. R. Saha, H. Sugawara, H. Sato, W. Higemoto, A. Koda, K. Ohishi, K. Nishiyama, and R. Kadono, Phys. Rev. Lett. **91**, 067003 (2003).
[14] G. M. Luke, Y. Fudamoto, K. M. Kojima, M. I. Larkin, J. Merrin, B. Nachumi, Y. J. Uemura, Y. Maeno, Z. Q. Mao, Y. Mori, H. Nakamura, and M. Sigrist, Nature (London) **396**, 658 (1998).
[15] A. D. Hillier, J. Quintanilla, B. Mazidian, J. F. Annett, and R. Cywinski, Phys. Rev. Lett. **109**, 097001 (2012).
[16] Y. Xing, H. Wang, C.-K. Li, X. Zhang, J. Liu, Y. Zhang, J. Luo, Z. Wang, Y. Wang, L. Ling, M. Tian, S. Jia, J. Feng, X.-J. Liu, J. Wei, and J. Wang, npj Quantum Mater. **1**, 16005 (2016).
[17] L. M. Schoop, L. S. Xie, R. Chen, Q. D. Gibson, S. H. Lapidus, I.r Kimchi, M. Hirschberger, N. Haldolaarachchige, M. N. Ali, C. A. Belvin, T. Liang, J. B. Neaton, N. P. Ong, A. Vishwanath, and R. J. Cava, Phys. Rev. B **91**, 214517 (2015).
[18] J.-F. Zhang, P.-J. Guo, M. Gao, K. Liu, and Z.-Y. Lu, Phys. Rev. B **99**, 045110 (2019).

[19] Y. Hattori, K. Fukamichi, T. Goto, and K. Suzuki, J. Phys. Soc. Jpn. **61**, 3845 (1992).
[20] T. Zhang, Y. Jiang, Z. Song, H. Huang, Y. He, Z. Fang, H. Weng, and C. Fang, Nature (London) **566**, 475 (2019).
[21] M. F. Gendron, R. E. Jones, J. Phys. Chem. Solids **23**, 405 (1962).
[22] Liang L. Zhao, Stefan Lausberg, H. Kim, M. A. Tanatar, Manuel Brando, R. Prozorov, and E. Morosan, Phys. Rev. B **85**, 214526 (2012).
[23] E. Svanidze and E. Morosan, Phys. Rev. B **85**, 174514 (2012).
[24] Y. Wang, H. Sato, Y. Toda, S. Ueda, H. Hiramatsu, and H. Hosono, Chem. Mater. **26**, 7209 (2014).
[25] D. C. Peets, E. Cheng, T. Ying, M. Kriener, X. Shen, S. Li, and D. Feng, Phys. Rev. B **99**, 144519 (2019).
[26] B. Lv, M. Li, J. Chen, Y. Yang, S. Wu, L. Qiao, F. Guan, H. Xing, Q. Tao, G.-H. Cao, and Z.-An. Xu, Phys. Rev. B **102**, 064507 (2020).
[27] H. Leng, J.-C. Orain, A. Amato, Y. K. Huang, and A. de Visser, Phys. Rev. B **100**, 224501 (2019).
[28] D. Singh, A. D. Hillier, and R. P. Singh, Phys. Rev. B **99**, 134509 (2019).
[29] J. Beare, M. Nugent, M. N. Wilson, Y. Cai, T. J. S. Munsie, A. Amon, A. Leithe-Jasper, Z. Gong, S. L. Guo, Z. Guguchia, Y. Grin, Y. J. Uemura, E. Svanidze, and G. M. Luke, Phys. Rev. B **99**, 134510 (2019).
[30] T. T. M. Palstra, G. Lu, A. A. Mcnovsky, G. J. Nieuwenhuys, P. H. Kes, and J. A. Mydosh, Phys. Rev. B **34**, 4566 (1986).
[31] V. K. Anand, D. Britz, A. Bhattacharyya, D. T. Adroja, A. D. Hillier, A. M. Strydom, W. Kockelmann, B. D. Rainford, and K. A. McEwen, Phys. Rev. B **90**, 014513 (2014).
[32] V. K. Anand, A. D. Hillier, D. T. Adroja, A. M. Strydom, H. Michor, K. A. McEwan, and B. D. Rainford, Phys. Rev. B **83**, 064522 (2011).
[33] R. Karl, F. Burri, A. Amato, M. Donegà, S. Gvasaliya, H. Luetkens, E. Morenzoni, and R. Khasanov, Phys. Rev. B **99**, 184515 (2019).
[34] A. Suter and B. M. Wojek, Phys. Procedia **30**, 69 (2012).
[35] E. E. Havinga, H. Damsma, and P. Hokkeling, J. Less-Common Met. **27**, 169 (1972).
[36] Z. Fisk and G. W. Webb, Phys. Rev. Lett. **36**, 1084 (1976).
[37] H. Wiesmann, M. Gurvitch, H. Lutz, A. K. Ghosh, B. Schwarz, M. Strongin, P. B. Allen, and J. W. Halley, Phys. Rev. Lett. **38**, 782 (1977).
[38] E. E. Havinga, H. Damsma, and P. Hokkeling, J. Less-Common Met. **27**, 281 (1972).
[39] T. Shibayama, M. Nohara, H. A. Katori, Y. Okamoto, Z. Hiroi, and H. Takagi, J. Phys. Soc. Jpn. **76**, 073708 (2007).
[40] D. Singh, J. A. T. Barker, A. Thamizhavel, D. McK. Paul, A. D. Hillier, and R. P. Singh, Phys. Rev. B **96**, 180501(R) (2017).
[41] W. L. McMillan, Phys. Rev. **167**, 331 (1968).
[42] D. Singh, A. D. Hillier, A. Thamizhavel, and R. P. Singh, Phys. Rev. B **94**, 054515 (2016).
[43] M. Tinkham, *Introduction to Superconductivity* (McGraw-Hill, New York, 1996).
[44] Y. J. Uemura, V. J. Emery, A. R. Moodenbaugh, M. Suenaga, D. C. Johnston, A. J. Jacobson, J. T. Lewandowski, J. H. Brewer, R. F. Kiefl, S. R. Kreitzman, G. M. Luke, T. Riseman, C. E. Stronach, W. J. Kossler, J. R. Kempton, X. H. Yu, D. Opie, and H. E. Schone, Phys. Rev. B **38**, 909(R) (1988).
[45] Y. J. Uemura, G. M. Luke, B. J. Sternlieb, J. H. Brewer, J. F. Carolan, W. N. Hardy, R. Kadono, J. R. Kempton, R. F. Kiefl, S. R. Kreitzman, P. Mulhern, T. M. Riseman, D. L. Williams, B. X. Yang, S. Uchida, H. Takagi, J. Gopalakrishnan, A. W. Sleight, M. A. Subramanian, C. L. Chien, M. Z. Cieplak, Gang Xiao, V. Y. Lee, B. W. Statt, C. E. Stronach, W. J. Kossler, and X. H. Yu, Phys. Rev. Lett. **62**, 2317 (1989).
[46] Y. J. Uemura, L. P. Le, G. M. Luke, B. J. Sternlieb, W. D. Wu, J. H. Brewer, T. M. Riseman, C. L. Seaman, M. B. Maple, M. Ishikawa, D. G. Hinks, J. D. Jorgensen, G. Saito, and H. Yamochi, Phys. Rev. Lett. **66**, 2665 (1991).